AGU ADVANCING EARTH AND SPACE SCIENCE

Geophysical Research Letters

RESEARCH LETTER
10.1029/2020GL090623

Late Miocene (10.0~6.0 Ma) Rapid Exhumation of the Chinese South Tianshan: Implications for the Timing of Aridification in the Tarim Basin

Jian Chang[1,2], Stijn Glorie[3], Nansheng Qiu[1,2], Kyoungwon Min[4], Yao Xiao[5], and Wei Xu[6]

[1]State Key Laboratory of Petroleum Resources and Prospecting, China University of Petroleum, Changping, BJ, China, [2]College of Geosciences, China University of Petroleum, Changping, BJ, China, [3]Department of Earth Sciences, the University of Adelaide, Adelaide, SA, Australia, [4]Department of Geological Sciences, University of Florida, Gainesville, FL, USA, [5]School of Earth and Environment Sciences, the University of Queensland, Brisbane, QLD, Australia, [6]Institute of Global Environmental Change, Xi'an Jiaotong University, Xi'an, SX, China

Abstract Cenozoic exhumation in the Tianshan is controlled by a complex interaction between tectonics and climate. However, the timing and magnitude of exhumation of the Tianshan and its contribution to climate change in Central Asia remains debated. In this study, we report new apatite fission track and (U-Th)/He ages for granite samples from the roof of the South Tianshan that are significantly younger than those published for other parts of the South Tianshan. Inverse and forward modeling reveals two phases of accelerated cooling at 10~6 Ma and since ~3 Ma, which can be linked to (1) the reactivation of strike-slip faults and hot asthenospheric upwelling during India-Eurasia convergence and (2) the interplay between tectonics and glaciation, respectively. The 10~6 Ma exhumation phase further corresponds to the timing of climate change, suggesting that this exhumation phase significantly contributed to the enhanced aridification of the Tarim Basin.

Plain Language Summary The tectonic uplift of the Mountains is closely related to climate change in nearby areas, e.g. the uplifting of the Tibetan Plateau plays an important on the aridification of the Tarim Basin since the Cenozoic. This study reported a new set of low-temperature thermochronological data from the high-elevation area of the Tianshan. They revealed the rapid exhumation of the central Chinese South Tianshan during 10.0-6.0 Ma, simultaneous with the enhanced aridification of the Tarim Basin. Therefore, we speculated that the uplift of the central South Tianshan have effectively blocked the humid westerlies from the Atlantic and Indian Oceans to enter the Tarim Basin and enhanced the aridification in the Tarim Basin during the late Miocene.

Key Points:

- We present a new set of AFT and AHe data for the Central South Tianshan, Central Asia.
- The Central South Tianshan experienced two phases of accelerated cooling occurred during 10~6 Ma and since ~3 Ma
- Rapid exhumation of the South Tianshan significantly contributed to the enhanced aridification of Tarim Basin during Late Miocene.

Supporting Information:

- Supporting Information S1

Correspondence to:
J. Chang,
changjian@cup.edu.cn

Citation:
Chang, J., Glorie, S., Qiu, N., Min, K., Xiao, Y., & Xu, W. (2021). Late Miocene (10.0~6.0 Ma) rapid exhumation of the Chinese South Tianshan: Implications for the timing of aridification in the Tarim Basin. *Geophysical Research Letters*, *48*, e2020GL090623. https://doi.org/10.1029/2020GL090623

Received 9 SEP 2020
Accepted 22 DEC 2020

1. Introduction

The Tianshan in Central Asia, is a classic example of an intracontinental mountain range that reactivated during the Cenozoic in response to the progressive collision between India and Eurasia (De Grave et al., 2007; Molnar & Tapponnier, 1975). Abundant low-temperature thermochronological studies have indicated that the Tianshan experienced punctuated denudation during the Meso-Cenozoic and accelerated exhumation since ~10 Ma (e.g., Glorie et al., 2011; Jepson et al., 2018a; Lü et al., 2020; Macaulay et al., 2014; Rolland et al., 2020). While low to moderate relief study areas predominantly record the Mesozoic denudation history of the Tianshan (e.g., De Grave et al., 2013; Gillespie et al., 2017; Glorie & De Grave, 2016; Glorie et al., 2010; Jolivet et al., 2010), recent studies have revealed that the granitic basement near fault zones in the highest mountains of the Tianshan (e.g., Peak Pobedi in Kyrgyzstan) as well as granitic clasts from modern moraines of the Tomor Glacier in China record younger apatite (U-Th)/He (AHe) ages within the range of 5.0~7.1 Ma (Jia et al., 2020; Rolland et al., 2020). Latter cooling ages correspond with the modelled timing of rapid deformation and exhumation (7~5.5 Ma) of the South Tianshan as revealed by magnetostratigraphy (J. M. Sun et al., 2009) and tectonic deformation studies of the Kuqa Fold-and-Thrust Belt (KFTB) (Hubert-Ferrari et al., 2007). However, the extent of the late Miocene exhumation of the South Tianshan is still poorly understood and direct low-temperature thermochronological evidence is scant. Given that young thermal histories have been recorded along the slopes of the highest mountains in the Tianshan

(Jia et al., 2020; Rolland et al., 2020), the central South Tianshan (CSTS), which hosts the highest elevation throughout the mountain range (Figure 1a), constitutes a promising area for researching the recent history of deformation and exhumation. In addition, the southern and northern sides of the South Tianshan show contrasting weather patterns, particularly during the summer, suggesting that moisture is effectively isolated in the north (i.e., the Yili Basin) of the South Tianshan, causing enhanced aridification in the south (i.e., the Tarim Basin) and forming the present-day Taklimakan Desert. Oxygen and carbon isotopes as well as magnetostratigraphic analyses suggest that enhanced aridification in the Tarim Basin initiated at 6∼5 Ma (Chang et al., 2012; J. M. Sun & Liu, 2006; J. M. Sun et al., 2017; Z. L. Zhang et al., 2020), which is possibly related to the uplift of the northern Tibetan Plateau (Chang et al., 2012; Fang et al., 2005) and the final collision between the Pamir and southwestern Tianshan (Heermance et al., 2018; Z. L. Zhang et al., 2020). However, the South Tianshan is geographically closer to the Tarim Basin and has, therefore, a greater potential to affect climate change within the Tarim Basin. Hence, in addition to contributing to our knowledge on the recent deformation history of the Tianshan, low-temperature thermochronology applied in the South Tianshan could shed more light on the diverging climate conditions that presumably initiated at 6∼5 Ma.

In this study, we report new AFT and AHe thermochronological data for seven samples collected from the southern flank of the CSTS (Figure 1b). AFT central ages, confined track lengths and single-grain AHe ages from volcanic and sedimentary outcrop samples were used for thermal history modeling, revealing important constraints on the timing and magnitude of exhumation in the South Tianshan. Furthermore, the potential driving forces for Neogene exhumation as well as the interplay between climate change and tectonic uplift in Central Asia are discussed.

2. Geological Setting and Previous Studies

The Tianshan in China consists of the Eastern and Western Tianshan, which are separated by the Urumqi-Korla line (Cai, 2000). The Western Tianshan is divided further into three domains by the Northern Tianshan Fault (NTSF) and South Tianshan Suture (STSs) (Figure 1a): The North, Central (including the Yili Block) and South Tianshan, with the latter hosting the study area for this work. The boundaries between the Central Tianshan, South Tianshan and the northern Tarim Basin are represented by two major faults: the STSs and North Tarim Fault (NTF), which developed at the southern margin of the South Tianshan (Figure 1a).

The CSTS is mainly composed of Mesoproterozoic to Permian metamorphic, volcanic, and clastic rocks and carbonates (Z. X. Zhu, 2006). The Tiereke Syncline, which exhibits a spectacular geomorphology with a slightly NW-SE inclined axial surface, is located along the northern margin of the KFTB (Figure 1b) and consists of Triassic-Miocene strata (lithologies and sediment thicknesses are provided in the supporting information: Text S1, Figures S3 and S4). Cenozoic crustal shortening and deformation in the South Tianshan and along the northern margin of the KFTB is generally considered to have initiated at 20∼25 Ma (A. Yin et al., 1998; Dumitru et al., 2001; X. Wang et al., 2011), after which deformation gradually propagated southward to the Qiulitag and Yaken anticlines in the south of KFTB at 7∼5 Ma (Figure 1a; Hubert-Ferrari et al., 2007; J. M. Sun et al., 2009; T. Zhang et al., 2014).

Several thermochrnological studies have attempted to reveal the exhumation history of the Tianshan. For the southern part of the Central Tianshan (close to the study area for this paper), relatively old AHe ages of 94∼161 Ma (in the Xiate profile) and 49∼201 Ma (in the Kekesu River profile) have been recorded (Yu et al., 2016), implying that the southern Central Tianshan may have been stable since the Paleogene. In addition, based on biotite $^{40}Ar/^{39}Ar$, zircon (U-Th)/He (ZHe), AFT and AHe data, Jolivet et al. (2010) and J. Yin et al. (2018) considered that the Central Tianshan experienced multiple cooling events during the Mesozoic and Cenozoic. The eastern margins of the Central and South Tianshan record AFT and AHe ages in the range from 35 Ma to 205 Ma (Du & Wang, 2007; Dumitru et al., 2001; Jolivet et al., 2010), while Miocene cooling was not documented in the thermochronological data-set. For the Eastern Tianshan, W. Zhu et al. (2006) and Yuan et al. (2007) reported a wide spectrum of AFT ages (12∼140 Ma), suggesting differential exhumation histories since the Early Cretaceous. In addition, Gillespie et al. (2017) proposed that the easternmost Tianshan experienced Early-Middle Triassic and Late Cretaceous cooling, while Cenozoic denudation in response to the collision of India with Eurasia has been insufficient to be detected

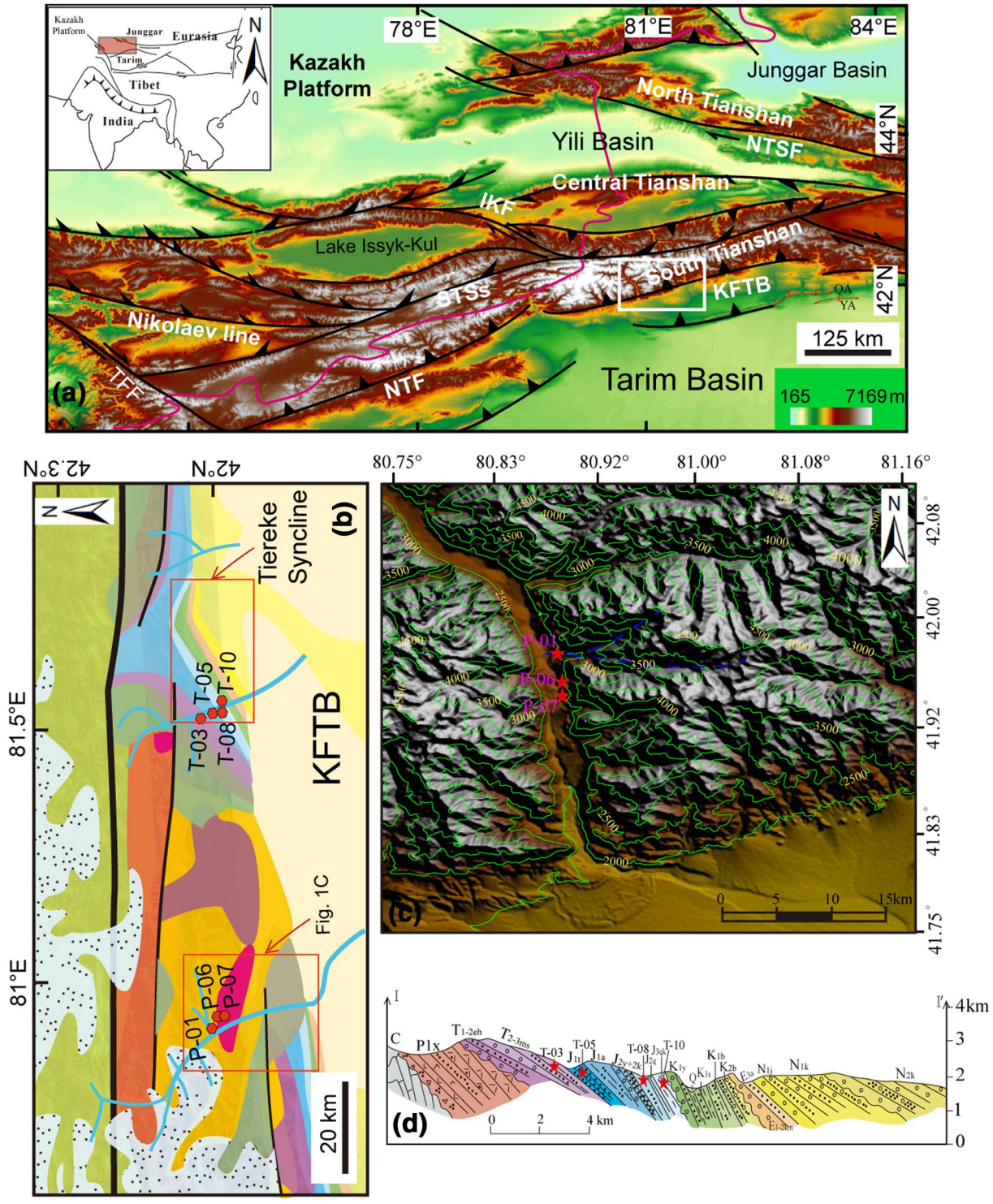

Figure 1. (a) General tectonic framework of the Tianshan with major faults. The studied area is circled by the white square. STSs: South Tianshan suture; IKF: Issyk-Kul Fault; TFF: Talas Fergana Fault; NTF: North Tarim Fault; NTSF: North Tianshan Fault; KFTB: Kuqa fold-and-thrust belt; QA: Qiulitag anticline; YA: Yaken anticline. (b) Geological map of the central part of the South Tianshan (modified from BGMRXUAR, 1989) indicating the locations of the samples with small red hexagons. (c) Geomorphology and elevation map near the samples P-01, P-06 and P-07 showing as red stars. The blue curves display the tributary of the Muzhaerte River, which provides provenance for sample P-01. (d) Typical cross-section (I-I') across the Mesozoic-Cenozoic strata near the Tiereke section showing the samples T-03, T-05, T-08 and T-10 with the red stars (modified from BGMRXUAR, 1982), which location is shown in Figure S3. The legend of Figures 1a, 1b and 1d is shown in Figure S2.

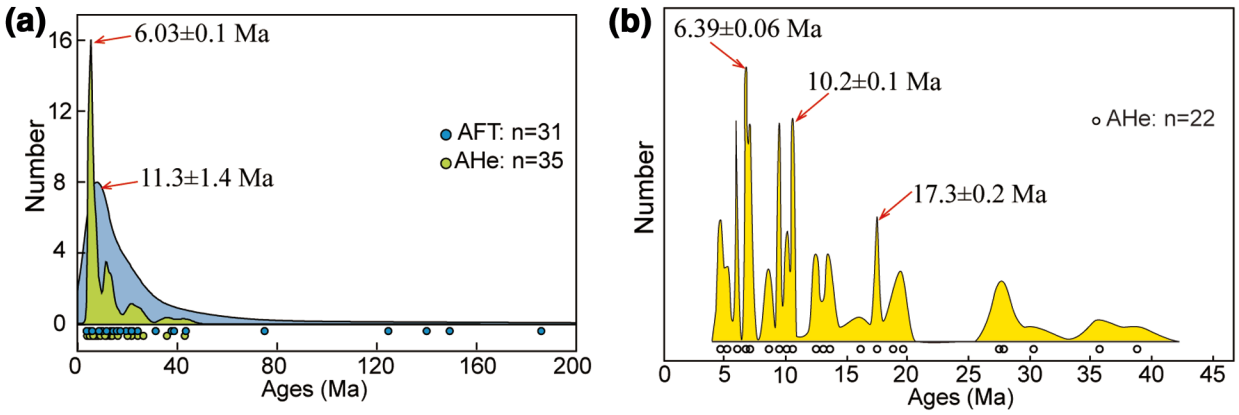

Figure 2. (a) Apatite fission-track (AFT) and (U-Th)/He (AHe) single-grain age histograms for sample P-01. (b) AHe single-grain histograms for the granite basement near the Peak Pobedi (Rolland et al., 2020).

by low-temperature thermochronology applied to surface samples. This study tests latter hypothesis using thermochronology applied to the roof of the Tianshan, where more extensive mountain building increases the likelihood to reveal Cenozoic exhumation.

3. Sample Information

In this study, seven samples were collected from the central South Tianshan (Table S1 in the supporting information). Sample P-01, an unconsolidated river sand sample, was collected from a tributary of the Muzhaerte River (Figures 1b and 1c). Samples P-06 and P-07 were obtained from Permian granitic outcrops (Figures 1b and 1c) near the Muzhaerte River that have only recently become accessible due to upgraded road conditions. In addition, the samples T-03, T-05, T-08 and T-10 were collected from the Triassic and Jurassic sedimentary strata near the Tiereke River (Figures 1b and 1c and S3), which belong to a part of the western limb of the Tiereke syncline. Both AFT and AHe data were collected from most samples with the exception of sample T-05 (AHe only) and sample T-08 (AFT only). The AHe and AFT data are presented in Tables S2 and S3. The thermal history modelling strategy involved (1) inverse modeling using the QTQt software (Gallagher, 2012), followed by (2) forward modeling using an in-house MATLAB script, which tests the inverse models against the apatite radiation damage accumulation and annealing model (RDAAM) and inheritance envelope concept, successively proposed by Flowers et al. (2009) and Guenthner et al. (2015). The detailed modeling parameters and procedures were described in Text S2 of the supporting information.

4. Low-temperature Thermochronology Data

Sample P-01 (unconsolidated river sand) yields scattered single-grain AHe and AFT ages, indicating that this sample represents a combination of numerous provenances characterized by different cooling ages. The AHe ages range from 4.2 ± 0.3 Ma to 43.0 ± 3.1 Ma and show a negatively (young) skewed distribution with a distinctive youngest peak at 6.03 ± 0.1 Ma (Figure 2a; Table S2). The AFT pooled age was calculated at 13.4 ± 1.1 Ma. Given that the $P(\chi^2)$ value for this sample is equal to 0 (Figure 2a; Table S3), the data was decomposed into age populations, with the youngest statistical AFT age population calculated at 11.3 ± 1.4 Ma.

The single-grain AHe ages for samples P-06 and P-07 show a slight positive correlation with eU contents (Figure 3c), implying that radiation damage might have an influence onto the AHe age dispersion. The weighted mean values of the single-grain AHe ages for samples P-06 and P-07 (Permian granite) are 4.59 ± 0.55 Ma and 5.38 ± 0.88 Ma, respectively. These ages correspond well with the youngest age population obtained from the river sand sample (6.03 ± 0.1 Ma; P-01) and for a basement granite intrusion (6.390

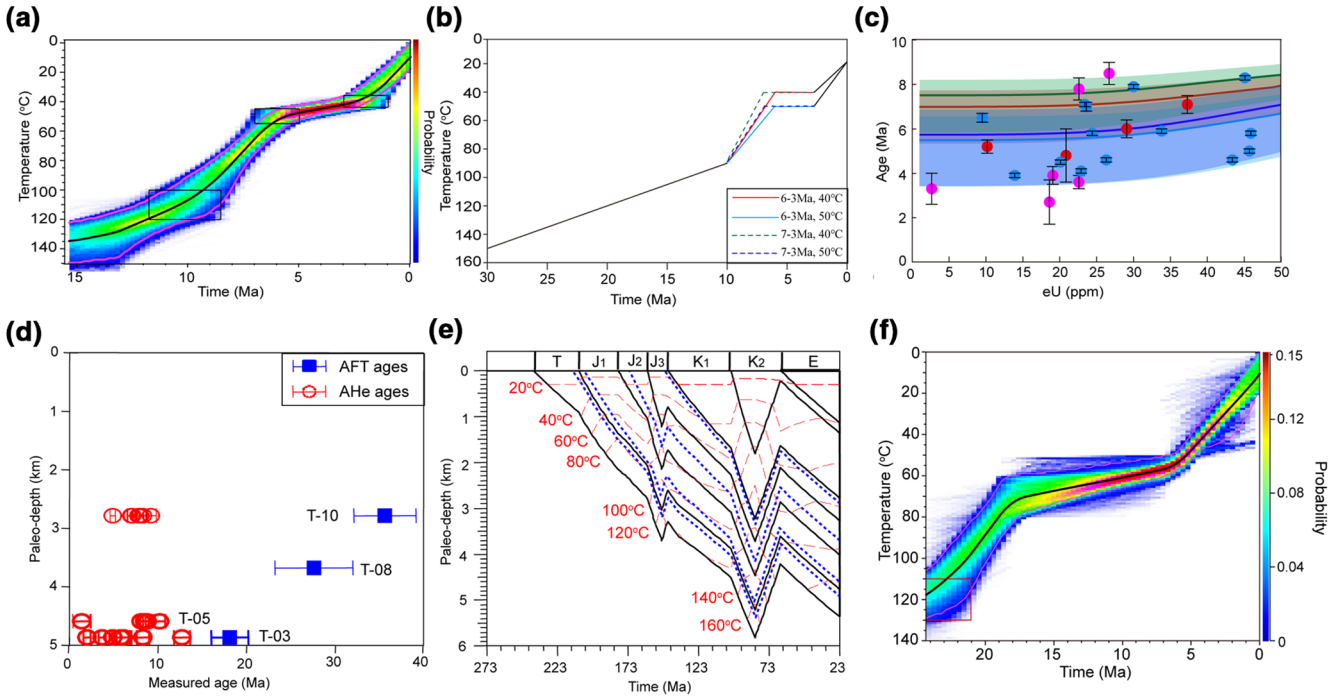

Figure 3. (a) Thermal history of sample P-06. The black line is the expected model, the magenta lines indicate 95% confidence intervals for the expected model, the color represents the path probability, and the black boxes are the constraints. (b) Temperature-time (t-T) paths for forward modeling; (c) Correlation between the single-grain AHe ages and eU for the samples P-06 and P-07 (red and purple circles) and presented by Jia et al. (2020) (light blue circles) with the inheritance envelopes taken from the modelled t-T paths in Figure 3b, the AHe ages with red circles were used for the inverse modeling in Figure 3a; (d) Apatite (AFT) and AHe ages vs. paleo-depth profiles for the samples from the Tiereke section, where the paleo-depths before the Miocene were calculated by the thicknesses of the residual strata (Figure S4). (e) Reconstructed burial and thermal history of the Tiereke section by utilizing the thicknesses of the residual strata and a steady-state heat flow model with a value of ~48 mW/m^2 (Figure S4; L. S. Wang et al., 2005). Blue dash-dotted lines represent the burial histories of samples T-03, T-05, T-08 and T-10 from deep to shallow depths. (f) Thermal history of sample T-03. The black line is the expected model, the magenta lines indicate 95% confidence intervals for the expected model, the color represents the path probability, and the red box is a constraint.

± 0.06 Ma) in the Kyrgyz Tianshan (Figure 2; Rolland et al., 2020). The AFT central ages of the samples P-06 and P-07 range from 10.5 ± 1.3 Ma to 11.3 ± 1.2 Ma, which are equal within uncertainty to the youngest AFT age population of P-01 (11.3 ± 1.4 Ma). Furthermore, the AFT central ages (10.1~10.3 Ma) and single-grain AHe age distribution (3.9~8.3 Ma) for the granite rocks from nearby modern moraines (Figure 3c; Jia et al., 2020) are in good agreement with those obtained for samples P-06 and P-07. Therefore, the Permian granite, near the highest mountains of the CSTS, is interpreted to have cooled through the AFT partial annealing zone and the AHe partial retention zone during the late Miocene and represents an important source for the youngest AHe and AFT age population of detrital sample P-01 and the modern moraine samples (Figures 1b and 1c). In order to reveal measurable confined fission tracks, samples P-06 and P-07 were exposed to ^{252}Cf irradiation at the University of Adelaide. However, given the very young AFT ages, only 15 confined tracks could be measured with a mean value of 13.4 ± 1.8 μm.

Samples T-03, T-05 and T-10 (sedimentary rocks) yielded single-grain AHe ages with weighted means of 6.9 ± 1.2 Ma, 8.8 ± 0.4 Ma and 7.7 ± 0.3 Ma, respectively. Regardless of their paleo-depths (Figure 3d), these tightly clustered weighted means suggest that their AHe systems were reset after deposition, thereby recording the timing of a late Miocene cooling event. Except for the sample T-10, the single-grain AHe ages for samples T-03 and T-05 display a positive relationship with eU contents (Figure S5). The AFT central ages for samples T-03, T-08 and T-10 range from 18.1 ± 2.1 Ma to 35.6 ± 3.5 Ma and become older as the paleo-depth decreases (Figure 3d), suggesting that these three samples experienced partial annealing during the Miocene. After ^{252}Cf irradiation, confined track lengths were measured, producing mean values of 12.6 ± 2.7 μm, 12.3 ± 2.7 μm and 14.1 ± 1.5 μm, respectively.

5. Thermal History Modeling

The two Permian granite samples (P-06 and P-07) were located only ~800 m apart horizontally and are, therefore, assumed to have experienced a similar thermal history. Here, sample P-06 was used to model the cooling history. According to the measured AFT central ages and single-grain AHe ages of the Permian granite in this study and presented by Jia et al. (2020), three constraint boxes of 110 ± 10°C at 10 ± 2 Ma, 50 ± 10°C at 6 ± 2 Ma and 40 ± 10°C at 4 ± 1 Ma were used in the thermal history modeling (Figure 3a). The QTQt modeling result indicate that sample P-06 firstly experienced a rapid cooling pulse between ~10 Ma and ~6.0 Ma, followed by a period of thermal quiescence from ~6.0 Ma to ~3.0 Ma, and finally rapid cooling again since ~3.0 Ma (Figure 3a). In order to quantitatively explain the dispersion of the single-grain AHe ages in this study and presented by Jia et al. (2020), forward modeling was carried out using a MATLAB script (Figures 3b and 3c). When the terminal time for the first rapid cooling was set at 6-7 Ma and the burial temperature from 6-7 Ma to 3 Ma was set to be 40~50°C, most single-grain AHe ages clustered into the inheritance envelope, indicating that the inversion result was credible.

Because the deformation of the northern margin of the KFTB gradually advanced southward during 20~25 Ma (Dumitru et al., 2001; X. Wang et al., 2011; A. Yin et al., 1998), the thermal histories of the Mesozoic samples from the Tiereke section were modeled separately (Figures 3e and 3f and S7). According to the thicknesses of the residual strata and the steady-state heat flow of ~48 mW/m^2 (L. S. Wang et al., 2005), the depth and temperature evolutions of the individual samples were reconstructed under the assumption that the sedimentary strata were horizontally distributed in the Tiereke section before the onset of Miocene deformation (Figure 3e). The QTQt modeling result for sample T-03 revealed rapid cooling during the early Miocene, followed by a very slow cooling at 70~55°C between ~18 Ma and ~6 Ma. A final phase of rapid cooling initiated at ~6.0 Ma (Figure 3f), and this pulse of rapid cooling is also detected in the thermal inversion result for sample T-08 (Figure S7).

6. Discussion and Conclusions

6.1. Dynamic Mechanism for Rapid Denudation Since ~10 Ma in the CSTS

The new modeling results in conjunction with previously reported thermochronological data suggest that the high relief CSTS records a young thermal history with rapid cooling during the Late Miocene (especially during ~10-6 Ma), which was previously reported in the Kyrgyz, Uzbek and Tajik Tianshan (Glorie et al., 2011; Jepson et al., 2018a, 2018b, and 2018c; Lü et al., 2020). This rapid late Miocene cooling event, identified in the CSTS, is supported by other lines of evidence, including field observations, seismic data, and regional tectonic settings, as discussed below. First, the collision between the Indian and Eurasian plates provided a large-scale tectonic framework that induced horizontal shortening and vertical movement (i.e., uplift) in the South Tianshan. Currently, the whole Western Tianshan continues to experience horizontal shortening at a rate of 4.7 ± 1.5 mm/yr, as estimated from GPS data. In addition, bending stresses from Tibetan loading also contributed to mountain building in the CSTS (Aitken, 2011; Figure 4a). It is worth noting that the CSTS has received more intense exhumation during ~10-6 Ma compared to other terranes in the southern Tianshan, although the shortening rate of the Tianshan decreases from the west to the east. Second, present-day GPS data and low-T thermochronological data imply that strike-slip faults throughout the Tianshan have been very active since the late Miocene (Figures S1b and S1c). As shown in Figures S1b and S1c, low-T thermochronological ages younger than ~10 Ma are mostly distributed near reactivated strike-slip faults in the Tianshan. Therefore, deformation of the CSTS since ~10-6 Ma was most likely related to superimposed NW-SE oriented compressional stresses (Wang & Li, 2007) generated by reactivated strike-slip faults including the IKF and STSs (Figure 1a). This phase of late Miocene reactivation is probably also responsible for the formation of the Tiereke syncline and related to the deformation of the Qiulitag and Yaken anticlines in the southern KFTB (Figures 1a and 4a; Hubert-Ferrari et al., 2007; J. M. Sun et al., 2009). The shortening rates in the KFTB increased rapidly to ~0.99 mm/yr, since ~6.5 Ma (T. Zhang et al., 2014). Third, the upwelling of hot asthenospheric mantle under the study area may have contributed to the observed rapid exhumation since the Late Miocene (Figure 4b; Lei & Zhao, 2007). During the late Miocene, convergence between the lithospheric blocks of the Tarim Basin and Junggar Basin (or the Kazakh Shield) caused the top section of the former to break off and sink (Figure 4b; Lei & Zhao, 2007), as indicated by

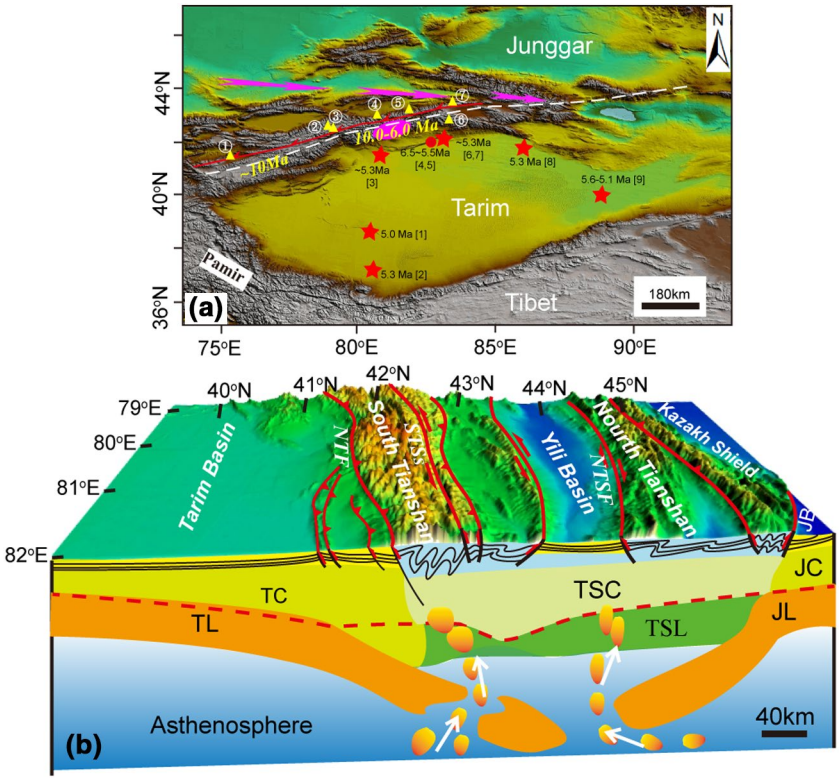

Figure 4. (a) Distribution of low-temperature thermochronological data in the central South Tianshan (CSTS) and adjacent areas and the enhanced aridification in the Tarim Basin. The pink arrows represent the prevailing wind direction of the Central Asia westerlies (Blomdin et al., 2016); the white dash-dot line indicates where bending stresses from Tibetan loading are interpreted to have focused mountain building within the Tianshan (Aitken, 2011). Yellow triangles show the locations of the AFT or AHe data along the STSs. ① is the Atbashi Range (Glorie et al., 2011); ② is the Sary-Dzhaz Range (Glorie et al., 2011); ③ is the granite intrusion near the Pobedi thrust (Rolland et al., 2020); ④ is the Xiate Profile; ⑤ is the Kekesu River Profile (Yu et al., 2016); ⑥ and ⑦ is the eastern part of the South Tianshan and Central Tianshan (Dumitru et al., 2001; J. Yin et al., 2018). Red stars represent the locations for the enhanced aridification research in the Tarim Basin. [1]-J. M. Sun et al. (2017); [2]-J. M. Sun and Liu (2006); [3]-Z. L. Zhang et al. (2020); [4,5]- Hubert-Ferrari et al. (2007) and J. M. Sun et al. (2009); [6,7]-Z. Q. Zhang and Sun (2011) and J. M. Sun et al. (2015); [8]-Z. C. Sun et al. (1999); [9]Chang et al. (2012); (b) Schematic illustration of the upwelling of deep asthenospheric materials under the Tianshan (modified from Lei & Zhao, 2007). TC-Tarim Basin crust; TL-Tarim Basin lithosphere; TSC-Tianshan crust; TSL-Tianshan lithosphere; JC-Junggar Basin crust; JL-Junggar Basin lithosphere; JB-Junggar Basin; NTF-North Tarim Fault; STSs- South Tianshan suture; NTSF-North Tianshan Fault.

seismic P-wave tomography. Light and hot asthenosphere may have begun upwelling following the sinking of the heavy Tarim Basin lithosphere, thereby triggering the rapid exhumation of the upper crust in the CSTS.

Southward thrusting of the South Tianshan became intense since ~6.0 Ma, which not resulted in the rapid deformation and exhumation of the southern margin of the Tianshan (Figure 3f), but formed the strata growth in the KFTB (J. M. Sun et al., 2009). Compared to the southern margin of the South Tianshan, the Permian granite in the CSTS experienced relatively slow cooling from ~6 Ma to ~3 Ma (Figure 3), which can be attributed to relative rock hardness and erodibility (Flowers & Ehlers, 2018). Granite is harder to erode than the sedimentary rocks, which can decelerate the denudation rate. Tectonic activity in the Tianshan accelerated since the Pliocene (~4-3 Ma), as demonstrated by increasing sedimentation and shortening rates (Charreau et al., 2008; Liavall et al., 2018; Tian et al., 2016), the widespread occurrence of Quaternary Xiyu conglomerates above unconformities (Charreau et al., 2009; Huang et al., 2010), and various thermochronological data (Bullen et al., 2003; Cao et al., 2013). Furthermore, during the late Pliocene and Pleistocene, the northern Hemisphere experienced enhanced glaciation (Martínez-Botí et al., 2015; Mudelsee & Raymo, 2005; Shackleton & Opdyke, 1977), which might have further accelerated bedrock denudation (Herman

et al., 2013; Thomson et al., 2010; P. Zhang et al., 2001). Hence, the interplay between tectonic activity and glaciation was probably responsible for the last phase of rapid exhumation of the CSTS since ~3 Ma.

6.2. Implications for Climate Change in the Tarim Basin

It has been suggested that enhanced aridification initiated in the Tarim Basin during 6~5 Ma (Figure 4a; Chang et al., 2012; J. M. Sun & Liu, 2006), which is coeval with the cease of the fastest phase of denudation in the CSTS and the onset of the last rapid cooling along the northern margin of the KFTB. Previous studies (Fang et al., 2005; Heermance et al., 2018; Jepson et al., 2018c; Z. L. Zhang et al., 2020) attributed this enhanced aridification to the tectonic uplift and deformation of the northern Tibetan Plateau and the final collision between the Pamir and Tianshan. Here, we speculate that the rapid exhumation in both the CSTS and the northern margin of the KFTB during 10~6 Ma most likely contributed to the enhanced aridification of the northern Tarim Basin. Based on the equations proposed by Brown (1991), England and Molnar (1990), and Tippett and Kamp (1993), we calculated that the elevation of the CSTS would have increased by >2,800m during this time period (see Text S3 of the supporting information), which could have effectively blocked the humid moisture (the westerlies) from the Atlantic and Indian Oceans to enter the Tarim Basin (Figure 4a; Blomdin et al., 2016; Cheng et al., 2012; X. Wang et al., 2020). The present-day Tianshan plays an important role in blocking humid air from circulating over the Tarim Basin, as evidenced by the contrast in the weather conditions between the southern and northern sides of the South Tianshan, particularly during the summer (Sorg et al., 2012). However, additional research is required to better understand the interplay between the tectonic uplift of the Tianshan and the aridification of the Tarim Basin.

Data Availability Statement

The AFT and AHe data in this study are available at the Mendeley Data website (http://dx.doi.org/10.17632/dc69bwyjsp.1)

Acknowledgments
This study was primarily supported by National Natural Science Foundation of China (41972125 and 41402112). SG's contributions were supported by an Australian Research Council Discovery Project (DP150101730). Comments from the anonymous reviewers and Editor Steve Jacobsen were helpful in improving the manuscript.

References

Aitken, A. R. A. (2011). Did the growth of Tibetan topography control the locus and evolution of Tien Shan mountain building? *Geology*, *39*, 459–462. https://doi.org/10.1130/g31712.1

Bureau of Geology and Mineral Resources of Xinjiang Uygur Autonomous Region (BGMRXUAR). (1982). *Geological map of the Quexiang area in the Xinjiang Uygur Autonomous Region at scale 1:200000*. Beijing: China Geological Map Press.

Bureau of Geology and Mineral Resources of Xinjiang Uygur Autonomous Region (BGMRXUAR). (1989). *Geological map of the Xinjiang Urgur Autonomous Region at scale 1:500000*. http://www.ngac.org.cn/Document/Map.aspx?MapId=EC7E1A7A75AC1954E0430100007F182E

Blomdin, R., Stroeven, A. P., Harbor, J. M., Lifton, N. A., Heyman, J., Gribenski, N., et al. (2016). Evaluating the timing of former glacier expansions in the Tian Shan: A key step toward robust spatial correlations. *Quaternary Science Reviews*, *153*, 78–96. https://doi.org/10.1016/j.quascirev.2016.07.029

Brown, R. W. (1991). Backstacking apatite fission-track "stratigraphy": A method for resolving the erosional and isostatic rebound components of tectonic uplift histories. *Geology*, *19*, 74–77. https://doi.org/10.1130/0091-7613(1991)019

Bullen, M. E., Burbank, D. W., & Garver, J. I. (2003). Building the Northern Tien Shan: integrated thermal, structural, and topographic constraints. *The Journal of Geology*, *111*, 149–165. https://doi.org/10.1086/345840

Cai, L. G. (2000). The transfer zone within intra-continent subduction orogenic belt in the Tian Shan, northwest China. *Experimental Petroleum Geology*, *22*, 206–209.(in Chinese with English abstract)

Cao, K., Bernet, M., Wang, G., van der Beek, P., Wang, A., Zhang, K., & Enkelmann, E. (2013). Focused Pliocene-Quaternary exhumation of the Eastern Pamir domes, western China. *Earth and Planetary Science Letters*, *363*, 16–26. https://doi.org/10.1016/j.epsl.2012.12.023

Chang, H., An, Z., Liu, W., Qiang, X., Song, Y., & Ao, H. (2012). Magnetostratigraphic and paleoenvironmental records for a late Cenozoic sedimentary sequence drilled from Lop Nor in the eastern Tarim Basin. *Global and Planetary Change*, *80–81*, 113–122. https://doi.org/10.1016/j.gloplacha.2011.09.008

Charreau, J., Avouac, J., Chen, Y., Dominguez, S., & Gilder, S. (2008). Miocene to present kinematics of fault-bend folding across the Huerguosi anticline, northern Tianshan (China), derived from structural, seismic, and magnetostratigraphic data. *Geology*, *36*(11), 871–874. https://doi.org/10.1130/g25073a.1

Charreau, J., Gumiaux, C., Avouac, J., Augier, R., Chen, Y., Barrier, L., et al. (2009). The Neogene Xiyu Formation, a diachronous prograding gravel wedge at front of the Tianshan: Climatic and tectonic implications. *Earth and Planetary Science Letters*, *287*, 298–310. https://doi.org/10.1016/j.epsl.2009.07.035

Cheng, H., Zhang, P. Z., Spötl, C., Edwards, R. L., Cai, Y. J., Zhang, D. Z., et al. (2012). The climatic cyclicity in semiarid-arid Central Asia over the past 500,000 years. *Geophysical Research Letters*, *39*, L01705. https://doi.org/10.1029/2011GL050202

De Grave, J., Buslov, M. M., & Van den haute, P. (2007). Distant effects of India–Eurasia convergence and Mesozoic intracontinental deformation in Central Asia: Constraints from apatite fission-track thermochronology. *Journal of Asian Earth Sciences*, *29*, 188–204. https://doi.org/10.1016/j.jseaes.2006.03.001

De Grave, J., Glorie, S., Buslov, M. M., Stockli, D. F., McWilliams, M. O., Batalev, V. Y., & Van den Haute, P. (2013). Thermo-tectonic history of the Issyk-Kul basement (Kyrgyz Northern Tien Shan, Central Asia). *Gondwana Research*, *23*, 998–1020. https://doi.org/10.1016/j.gr.2012.06.014

Dumitru, T. A., Zhou, D., Chang, E. Z., Graham, S. A., Hendrix, M. S., Sobel, E. R., & Carroll, A. R. (2001). Uplift, exhumation, and deformation in the Chinese Tian Shan. In M. S. Hendrix, & G. A. Davis (Eds.), Paleozoic and mesozoic tectonic evolution of central Asia: From continental assembly to intracontinental deformation: Boulder, Colorado. Vol. 194 (pp. 71–99) Geological Society of America Memoir.

Du, Z. L., & Wang, Q. C. (2007). Mesozoic and Cenozoic uplifting history of the Tianshan Region: Insight from apatite fission track. *Acta Geologica Sinica*, *81*, 1081–1101 (in Chinese with English abstract).

England, P., & Molnar, P. (1990). Surface uplift, uplift of rocks, and exhumation of rocks. *Geology*, *18*, 1173–1177. https://doi.org/10.1130/0091-7613(1990)018

Fang, X. M., Yan, M. D., Van der Voo, R., Rea, D. K., Song, C. H., Pares, J. M., et al. (2005). Late Cenozoic deformation and uplift of the NE Tibetan Plateau: Evidence from high-resolution magnetostratigraphy of the Guide Basin, Qinghai Province, China. *GSA Bulletin*, *117*, 1208–1225. https://doi.org/10.1130/B25727.1

Flowers, R. M., & Ehlers, T. A. (2018). Rock erodibility and the interpretation of low-temperature thermochronologic data. *Earth and Planetary Science Letters*, *482*, 312–323. https://doi.org/10.1016/j.epsl.2017.11.018

Flowers, R. M., Ketcham, R. A., Shuster, D. L., & Farley, K. A. (2009). Apatite (U-Th)/He thermochronometry using a radiation damage accumulation and annealing model. *Geochimica et Cosmochimica Acta*, *73*, 2347–2365. https://doi.org/10.1016/j.gca.2009.01.015

Gallagher, K. (2012). Transdimensional inverse thermal history modeling for quantitative thermochronology. *Journal of Geophysical Research*, *117*, B02408. https://doi.org/10.1029/2011JB008825

Gillespie, J., Glorie, S., Xiao, W., Zhang, Z., Collins, A. S., Evans, N., et al. (2017). Mesozoic reactivation of the Beishan, southern Central Asian Orogenic Belt: Insights from low-temperature thermochronology. *Gondwana Research*, *43*, 107–122. https://doi.org/10.1016/j.gr.2015.10.004

Glorie, S., & De Grave, J. (2016). Exhuming the Meso-Cenozoic Kyrgyz Tianshan and Siberian Altai-Sayan: A review based on low-temperature thermochronlogy. *Geoscience Frontiers*, *7*, 155–170. https://doi.org/10.1016/j.gsf.2015.04.003

Glorie, S., De Grave, J., Buslov, M. M., Elburg, M. A., Stockli, D. F., Gerdes, A., & Van den haute, P. (2010). Multi-method chronometric constraints on the evolution of the Northern Kyrgyz Tien Shan granitoids (Central Asian Orogenic Belt): from emplacement to exhumation. *Journal of Asian Earth Sciences*, *38*, 131–146. https://doi.org/10.1016/j.jseaes.2009.12.009

Glorie, S., De Grave, J., Buslov, M. M., Zhimulev, F. I., Stockli, D. F., Batalev, V. Y., et al. (2011). Tectonic history of the Kyrgyz South Tien Shan (Atbashi-Inylchek) suture zone: The role of inherited structures during deformation-propagation. *Tectonics*, *30*, TC6016. https://doi.org/10.1029/2011TC002949

Guenthner, W. R., Reiners, P. W., DeCelles, P. G., & Kendall, J. (2015). Sevier belt exhumation in central UT constrained from complex zircon (U-Th)/He data sets: Radiation damage and He inheritance effects on partially reset detrital zircons. *GSA Bulletin*, *127*, 323–348. https://doi.org/10.1130/B31032.1

Heermance, R. V., Pearson, J., Moe, A., Liu, L., Xu, J., Chen, J., et al. (2018). Erg deposition and development of the ancestral Taklimakan Desert (western China) between 12.2 and 7.0 Ma. *Geology*, *46*, 919–922. https://doi.org/10.1130/G45085.1

Herman, F., Seward, D., Valla, P. G., Carter, A., Kohn, B., Willett, S. D., & Ehlers, T. A. (2013). Worldwide acceleration of mountain erosion under a cooling climate. *Nature*, *504*, 423–426. https://doi.org/10.1038/nature12877

Huang, B., Piper, J. D. A., Qiao, Q., Wang, H., & Zhang, C. (2010). Magnetostratigraphic and rock magnetic study of the Neogene upper Yaha section, Kuche Depression (Tarim Basin): Implications to formation of the Xiyu conglomerate formation, NW China. *Journal of Geophysical Research*, *115*, B01101. https://doi.org/10.1029/2008JB006175

Hubert-Ferrari, A., Suppe, J., Gonzalez-Mieres, R., & Wang, X. (2007). Mechnisms of active folding of the landscape (southern Tian Shan, China). *Journal of Geophysicsl Research*, *112*, B03S09. https://doi.org/10.1029/2006JB004362

Izquierdo-Liavall, E., Roca, E., Xie, H., Pla, O., Muñoz, J. A., Rowan, M. G., et al. (2018). Influence of overlapping décollements, syntectonic sedimentation, and structural inheritance in the evolution of a contractional system: The central Kuqa fold-and-thrust belt (Tian Shan mountains, NW China). *Tectonics*, *37*, 2608–2632. https://doi.org/10.1029/2017TC004928

Jepson, G., Glorie, S., Konopelko, D., Gillespie, J., Danisik, M., Evans, N. J., et al. (2018a). Thermochronological insights into the structural contact between the Tian Shan and Pamirs, Tajikistan. *Terra Nova*, *30*, 95–104. https://doi.org/10.1111/ter.12313

Jepson, G., Glorie, S., Konopelko, D., Gillespie, J., Danišík, M., Mirkamalov, R., et al. (2018b). Low-temperature thermochronology of the Chatkal-Kurama Terrane: Insights into the Meso-Cenozoic thermal history of the Western Tian Shan. *Tectonics*, *37*(10), 3954–3969. https://doi.org/10.1029/2017TC004878

Jepson, G., Glorie, S., Konopelko, D., Mirkamalov, R., Danišík, M., & Collins, A. S. (2018c). The low-temperature thermo-tectonic evolution of the western Tian Shan, Uzbekistan. *Gondwana Research*, *64*, 122–136. https://doi.org/10.1016/j.gr.2018.08.003

Jia, Y. Y., Sun, J. M., Lü, L. X., Pang, J. Z., & Wang, Y. (2020). Late Oligocene-Miocene intra-continental mountain building of the Harke Mountains, southern Chinese Tian Shan: Evidence from detrital AFT and AHe analysis. *Journal of Asian Earth Sciences*, *191*, 104198. https://doi.org/10.1016/j.jseaes.2019.104198

Jolivet, M., Dominguez, S., Charreau, J., Chen, Y., Li, Y. A., & Wang, Q. C. (2010). Mesozoic and Cenozoic tectonic history of the central Chinese Tian Shan: Reactivated tectonic structures and active deformation. *Tectonics*, *29*, TC6019. https://doi.org/10.1029/2010TC002712

Lei, J. S., & Zhao, D. P. (2007). Teleseismic P-wave tomography and the upper mantle structure of the central Tien Shan orogenic belt. *Physics of the Earth and Planetary Interiors*, *162*, 165–185. https://doi.org/10.1016/j.pepi.2007.04.010

Lü, L., Sun, J., Zhang, Z., Jia, Y., Tian, S., Abdulov, S., et al. (2020). Late Miocene accelerated exhumation in the central Tajik Basin and implications for northward indention and lateral growth of the Pamir. *Tectonopysics*, *787*, 228438. https://doi.org/10.1016/j.tecto.2020.228438

Macaulay, E. A., Sobel, E. R., Mikolaichuk, A., Kohn, B., & Stuart, F. M. (2014). Cenozoic deformation and exhumation history of the Central Kyrgyz Tien Shan. *Tectonics*, *33*, 135–165. https://doi.org/10.1002/2013TC003376

Martínez-Botí, M. A., Foster, G. L., Chalk, T. B., Rohling, E. J., Sexton, P. F., Lunt, D. J., et al. (2015). Plio-Pleistocene climate sensitivity evaluated using high-resolution CO_2 records. *Nature*, *518*, 49–54. https://doi.org/10.1038/nature14145

Molnar, P., & Tapponnier, P. (1975). Cenozoic Tectonics of Asia: Effects of a continental collision. *Science*, *189*, 419–426. https://doi.org/10.1126/science.189.4201.419

Mudelsee, M., & Raymo, M. E. (2005). Slow dynamics of the Northern Hemisphere glaciation. *Paleoceanography*, *20*, 1–14. https://doi.org/10.1029/2005PA001153

Rolland, Y., Jourdon, A., Petit, C., Bellahsen, N., Loury, C., Sobel, E. R., & Glodny, J. (2020). Thermochronology of the highest central Asian massifs (Khan Tengri-Pobedi, SE Kyrgyztan): Evidence for Late Miocene (ca. 8 Ma) reactivation of Permian faults and insights into building the Tian Shan. *Journal of Asian Earth Sciences*, *200*, 104466. https://doi.org/10.1016/j.jseaes.2020.104466

Shackleton, N. J., & Opdyke, N. D. (1977). Oxygen isotope and paleomagnetic evidence for early Northern Hemisphere glaciation. *Nature*, *270*, 216–219. https://doi.org/10.1038/270216a0

Sorg, A., Bolch, T., Stoffel, M., Solomina, O., & Beniston, M. (2012). Climate change impacts on glaciers and runoff in Tien Shan (Central Asia). *Nature Climate Change*, *v. 2*, 725–731. https://doi.org/10.1038/NCLIMATE1592

Sun, Z. C., Feng, X. J., Li, D. M., Yang, F., Qu, Y. H., & Wang, H. J. (1999). Cenozoic ostracoda and palaeoenvironments of the northeastern Tarim Basin, western China. *Palaeogeography, Palaeoclimatology, Palaeoecology*, *148*, 37–50. https://doi.org/10.1016/S0031-0182(98)00174-6

Sun, J. M., Gong, Z. J., Tian, Z. H., Jia, Y. Y., & Windley, B. (2015). Late Miocene stepwise aridification in the Asian interior and the interplay between tectonics and climate. *Palaeogeography, Palaeoclimatology, Palaeoecology*, *421*, 48–59. https://doi.org/10.1016/j.palaeo.2015.01.001

Sun, J. M., & Liu, T. S. (2006). The age of the Taklimakan Desert. *Science*, *312*, 1621. https://doi.org/10.1126/science.1124616

Sun, J. M., Liu, W. G., Liu, Z. H., Deng, T., Windley, B. F., & Fu, B. H. (2017). Extreme aridification since the beginning of the Pliocene in the Tarim Basin, western China. *Palaeogeography, Palaeoclimatology, Palaeoecology*, *485*, 189–200. https://doi.org/10.1016/j.palaeo.2017.06.012

Sun, J. M., Li, Y., Zhang, Z. Q., & Fu, B. H. (2009). Magnetostratigraphic data on Neogene growth folding in the foreland basin of the southern Tianshan Mountains. *Geology*, *37*, 1051–1054. https://doi.org/10.1130/g30278a.1

Thomson, S. N., Brandon, M. T., Tomkin, J. H., Reiners, P. W., Vásquez, C., & Wislon, N. J. (2010). Glaciation as a destructive and constructive control on mountain building. *Nature*, *467*, 313–317. https://doi.org/10.1038/nature09365

Tian, Z., Sun, J., Windley, B. F., Zhang, Z., Gong, Z., Lin, X., & Xiao, W. (2016). Cenozoic detachment folding in the southern Tianshan foreland, NW China: Shortening distances and rates. *Journal of Structural Geology*, *84*, 142–161. https://doi.org/10.1016/j.jsg.2016.01.007

Tippett, J. M., & Kamp, P. J. J. (1993). Fission track analysis of the late Cenozoic vertical kinematics of continental Pacific crust, South Island, New Zealand. *Journal of Geophysical Research*, *98*, 16119–16148. https://doi.org/10.1029/92JB02115

Wang, X., Carrapa, B., Sun, Y., Dettman, D. L., Chapman, J. B., Rugenstein, J. K. C., et al. (2020). The role of the westerlies and orography in Asian hydroclimate since the late Oligocene. *Geology*, *48*, 728–732. https://doi.org/10.1130/G47400.1

WangQ. C., & LiZ. (Eds.). (2007). *Basin-mountain system between Kuqa and Tianshan and its implication for hydrocarbon accumulation* (pp. 113). Science Press (in Chinese).

Wang, L. S., Li, C., Liu, S. W., Li, H., Xu, M. J., Yu, D. Y., et al. (2005). Terrestrial heat flow distribution in Kuqa foreland basin, Tarim, NW China. *Petroleum Exploration and Development*, *32*, 79–83 (in Chinese with English abstract).

Wang, X., Suppe, J., Guan, S. W., Hubert-Ferrari, A., Gonzalez-Mieres, R., & Jia, C. Z. (2011). Cenozoic structure and tectonic evolution of the Kuqa fold belt, southern Tianshan, China. In K. McClay, J. H. Shaw, & J. Suppe (Eds.), Thrust fault-related folding (Vol. 94, pp. 215–243). AAPG Memoir. https://doi.org/10.1306/13251339M94389

Wang, Q., Zhang, P. Z., Freymueller, J. T., Bilham, R., Larson, K. M., Lai, X. A., et al. (2001). Present-day crustal deformation in China constrained by global positioning system measurements. *Sciences*, *294*, 574–577. https://doi.org/10.1126/science.1063647

Yin, J., Chen, W., Hodges, K. V., Xiao, W., Cai, K., Yuan, C., et al. (2018). The thermal evolution of Chinese central Tianshan and its implications: Insights from multi-method chronometry. *Tectonophysics*, *722*, 536–548. https://doi.org/10.1016/j.tecto.2017.11.037

Yin, A., Nie, S., Craig, P., Harrision, T. M., Ryerson, F. J., Qian, X. L., & Yang, G. (1998). Late Cenozoic tectonic evolution of the southern Chinese Tian Shan. *Tectonics*, *17*, 1–27. https://doi.org/10.1029/97TC03140

Yuan, W., Bao, Z., Dong, J., Guo, Z., & Deng, J. (2007). Fission track analysis of tectonic activity and mineralization epoch in the Tuwu-Yandong porphyry copper deposit, Xinjiang. *Science China Earth Sciences*. 1330–1337. (in Chinese).

Yu, S., Chen, W., Zhang, B., Sun, J. B., Li, C., Yuan, X., et al. (2016). Mesozoic and Cenozoic uplift and exhumation history of the Kekesu section in the Center Tianshan: Constrained from (U-Th)/He thermochronometry. *Chinese Journal of Geophysics*, *59*, 2922–2936. https://doi.org/10.6038/cjg20160817. (in Chinese).

Zhang, T., Fang, X. M., Song, C. H., Appel, E., & Wang, Y. D. (2014). Cenozoic tectonic deformation and uplift of the South Tian Shan: Implications from magnetostratigraphy and balanced cross-section restoration of the Kuqa depression. *Tectonophysics*, *628*, 172–187. https://doi.org/10.1016/j.tecto.2014.04.044

Zhang, P., Molnar, P., & Downs, W. R. (2001). Increased sedimentation rates and grain sizes 2-4 Myr ago due to the influence of climate change on erosion rates. *Nature*, *410*, 891–897. https://doi.org/10.1038/35073504

Zhang, Z. Q., & Sun, J. M. (2011). Palynological evidence for Neogene environmental change in the foreland basin of the southern Tianshan range, northwestern China. *Global and Planetary Change*, *75*, 56–66. https://doi.org/10.1016/j.gloplacha.2010.10.006

Zhang, Z. L., Sun, J. M., Tian, S. C., Lü, L. X., Su, B., Cao, M. M., et al. (2020). Environmental magnetic evidence for enhanced aridification in the Tarim Basin since ~5.3 Ma, NW China. *Journal of Asian Earth Sciences*, *189*, 104181. https://doi.org/10.1016/j.jseaes.2019.104181

Zhu, W., Shu, L., Wan, J., Sun, Y., Wang, F., & Zhao, Z. (2006). Fission-track evidence for the exhumation history of Bogda-Harlik Mountains, Xinjiang since the Cretaceous. *Acta Geologica Sinica*, *80*, 16–22 (in Chinese with English abstract).

Zhu, Z. X. (2006). The Geological components and tectonic evolution of South Tianshan. Xinjiang (PhD thesis). Beijing, Chinese Academy of Geological Sciences (pp. 29) In Chinese with English abstract.

References from the Supporting Information

Chang, J., Tian, Y. T., & Qiu, N. S. (2017). Mid-Late Miocene deformation of the northern Kuqa fold-and-thrust belt (southern Chinese Tian Shan): An apatite (U-Th-Sm)/He study. *Tectonophysics*, *694*, 101–113. https://doi.org/10.1016/j.tecto.2016.12.003

Chen, Z. L., Li, L., Liu, J., Gong, H. L., Jiang, R. B., Li, S. X., et al. (2008). Preliminary study on the uplifting-exhumation process on the western Tianshan range, northwestern China. *Acta Petrologica Sinica*, *24*, 625–636. (in Chinese with English abstract).

Chen, Z. L., Wan, J. L., Liu, J., Li, S. X., Zhen, E. J., Han, X. Z., et al. (2006). Multi-stage uplift and exhumation of the West Tianshan Mountain: Evidence from the apatite fission-track dating. *Acta Geoscientica Sinica*, *27*, 97–106. (in Chinese with English abstract).

De Grave, J., Glorie, S., Buslov, M. M., Izmer, A., Fournier-Carrie, A., Batalev, V. Y., et al. (2011). The thermo-tectonic history of the Song-Kul plateau, *Kyrgyz Tien Shan: Constraints by apatite and titanite thermochronometry and zircon U/Pb dating. Gondwana Research*, *20*, 745–763. https://doi.org/10.1016/j.gr.2011.03.011

De Grave, J., Glorie, S., Ryabinin, A., Zhimulev, F., Buslov, M. M., Izmer, A., et al. (2012). Late Palaeozoic and Meso-Cenozoic tectonic evolution of the southern Kyrgyz Tien Shan: Constraints from multi-method thermochronology in the Trans-Alai, Turkestan-Alai segment and the southeastern Ferghana Basin. *Journal of Asian Earth Sciences*, *44*, 149–168. https://doi.org/10.1016/j.jseaes.2011.04.019

Donelick, R. A., O'Sullivan, P. B., & Ketcham, R. A. (2005). *Apatite fission-track analysis. Reviews in Mineralogy and Geochemistry*, 58, 49–94. https://doi.org/10.2138/rmg.2005.58.3

Dunkl, I. (2002). Trackkey: a windows program for calculation and graphical presentation of fission track data. *Computers & Geosciences*, *28*, 3–12. https://doi.org/10.1016/S0098-3004(01)00024-3

Farley, K. A., Wolf, R. A., & Silver, L. T. (1996). The effects of long alpha-stopping distances on (U-Th)/He ages. *Geochimica et Cosmochimica Acta*, *60*, 4223–4229. https://doi.org/10.1016/S0016-7037(96)00193-7

Galbraith, R. F. (1981). On statistical models for fission track counts. *Journal of the International Association for Mathematical Geology*, *13*, 471–478. https://doi.org/10.1007/BF01034498

Gallagher, K., Charvin, K., Nielsen, S., Sambridge, M., & Stephenson, J. (2009). Markov chain Monte Carlo (MCMC) sampling methods to determine optimal models, model resolution and model choice for earth science problems. *Marine and Petroleum Geology*, *26*, 525–535. https://doi.org/10.1016/j.marpetgeo.2009.01.003

Guo, Z. J., Zhang, Z. C., Wu, C. D., Fang, S. H., & Zhang, R. (2006). The Mesozoic and Cenozoic exhumation history of Tianshan and comparative studies to the Junggar and Altai Mountains. *Acta Geologica Sinica*, *80*, 1–15. (in Chinese with English abstract).

Ketcham, R. A., Carter, A., Donelick, R. A., Barbarand, J., & Hurford, A. J. (2007). Improved modeling of fission-track annealing in apatite. *American Mineralogist*, *92*, 799–810. https://doi.org/10.2138/am.2007.2281

Li, Z., & Peng, S. T. (2010). Detrital zircon geochronology and its provenance implications: Responses to Jurassic through Neogene basin-range interactions along northern margin of the Tarim Basin, Northwest China. *Basin Research*, *22*, 126–138. https://doi.org/10.1111/j.1365-2117.2009.00440.x

Macaulay, E. A., Sobel, E. R., Mikolaichuk, A., Landgraf, A., Kohn, B., & Stuart, F. (2013). Thermochronologic insight into late Cenozoic deformation in the basement-cored Terskey range. *Kyrgyz Tien Shan: Tectonics*, *32*, 487–500. https://doi.org/10.1002/tect.20040

Métivier, F., & Gaudemer, Y. (1997). MA transfer between eastern Tien Shan and adjacent basins (central Asia): Constraints on regional tectonics and topography. *Geophysical Journal International*, *128*(1), 1–17. https://doi.org/10.1111/j.1365-246X.1997.tb04068.x

Sobel, E. R., Chen, J., & Heermance, R. V. (2006). Late Oligocene-Early Miocene initiation of shortening in the Southwestern Chinese Tian Shan: Implications for Neogene shortening rate variations. *Earth and Planetary Science Letters*, *247*, 70–81. https://doi.org/10.1016/j.epsl.2006.03.048

Sobel, E. R., & Dumitru, T. A. (1997). Thrusting and exhumation around the margins of the western Tarim Basin during the India-Asia collision. *Journal of Geophysical Research*, *102*, 5043–5063. https://doi.org/10.1029/96JB03267

Sobel, E. R., Oskin, M., Burbank, D., & Mikolaichuk, A. (2006). Exhumation of basement-cored uplifts: Example of the Kyrgyz Range quantified with apatite fission track thermochronology. *Tectonics*, *25*, 2008. https://doi.org/10.1029/2005TC001809

Vogl, J. J., Min, K., Carmenate, A., Foster, D. A., & Marsellos, A. (2014). Miocene regional hotspot-related uplift, exhumation, and extension north of the Snake River Plain: Evidence from apatite (U-Th)/He thermochronology. *Lithosphere*, *6*, 108–123. https://doi.org/10.1130/L308.1

Zhang, B., Chen, W., Sun, J. B., Yu, S., Yin, J. Y., Li, J., et al. (2016). The thermal history and uplift process of the Ouxidaban pluton in the South Tianshan orogen: Evidence from Ar-Ar and (U-Th)/He. *Science China: Earth Sciences*, *59*, 349–361. https://doi.org/10.1007/s11430-015-5218-z

Zhang, Z. Y., Zhu, W. B., Shu, L. S., Wan, J. L., Yang, W., Su, J. B., & Zheng, B. H. (2009). Apatite fission track thermochronology of the Precambrian Aksu blueschist, NW China: Implications for thermo-tectonic evolution of the north Tarim Basement. *Gondwana Research*, *16*, 182–188. https://doi.org/10.1016/j.gr.2009.04.006